ACS chemical biology

Letters

pubs.acs.org/acschemicalbiology

CRISPR–Cas9 Mediated DNA Unwinding Detected Using Site-Directed Spin Labeling

Narin S. Tangprasertchai,[†] Rosa Di Felice,[‡,§,∥] Xiaojun Zhang,[†] Ian M. Slaymaker,[⊥] Carolina Vazquez Reyes,[†] Wei Jiang,[†] Remo Rohs,[†,‡,§] and Peter Z. Qin*[,†,§]

[†]Department of Chemistry, [‡]Department of Physics and Astronomy, and [§]Department of Biological Sciences, University of Southern California, Los Angeles, California 90089, United States

[∥]Center S3, CNR Institute of Nanoscience, Via Campi 213/A, 41125 Modena, Italy

[⊥]Broad Institute of MIT and Harvard, Cambridge, Massachusetts 02142, United States

Supporting Information

ABSTRACT: The RNA-guided CRISPR–Cas9 nuclease has revolutionized genome engineering, yet its mechanism for DNA target selection is not fully understood. A crucial step in Cas9 target recognition involves unwinding of the DNA duplex to form a three-stranded R-loop structure. Work reported here demonstrates direct detection of Cas9-mediated DNA unwinding by a combination of site-directed spin labeling and molecular dynamics simulations. The results support a model in which the unwound nontarget strand is stabilized by a positively charged patch located between the two nuclease domains of Cas9 and reveal uneven increases in flexibility along the unwound nontarget strand upon scissions of the DNA backbone. This work establishes the synergistic combination of spin-labeling and molecular dynamics to directly monitor Cas9-mediated DNA conformational changes and yields information on the target DNA in different stages of Cas9 function, thus advancing mechanistic understanding of CRISPR–Cas9 and aiding future technological development.

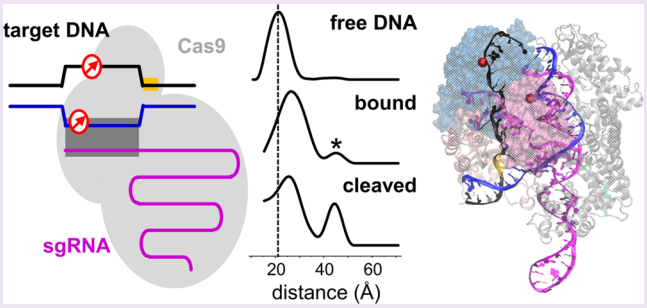

Clustered regularly interspaced short palindromic repeats (CRISPR) and CRISPR-associated (Cas) proteins constitute a class of adaptive immunity systems used by bacteria and archaea to combat invading viruses and other mobile genetic elements.[1−3] In type II CRISPR–Cas systems, a single Cas9 protein is activated by CRISPR-encoded small RNAs to cleave double-stranded DNA at sites determined by the complementarity between a single-stranded region of the RNA and a segment of the target DNA (designated as the protospacer), as well as a short protospacer-adjacent motif (PAM) within the target DNA.[4,5] Substituting the native small RNAs with a single-guide RNA (sgRNA) generates a programmable Cas9 to target precise DNA sequences in many cell types,[4,6,7] which has led to a revolution in genome engineering.[8,9]

Understanding the mechanism of DNA recognition used by Cas9 is critical for further developing this powerful tool for genome engineering.[8,9] Intensive studies, the majority of which focus on the *Streptococcus pyogenes* Cas9, have led to a proposed mechanism in which multiple, large scale conformational changes of Cas9, guided and coordinated by both RNA and DNA, discriminate between correct and incorrect targets.[10−19] Among these, a key step is unwinding of the DNA duplex to form a stable R-loop structure, in which the guide segment of the RNA is duplexed with the target strand of the DNA, while the DNA nontarget strand is unpaired. Information on the R-loop and the unwound DNA is important not only in dissecting Cas9 function but also in developing Cas9-based technology, as evident by the success in engineering Cas9 variants with greatly enhanced specificity[20−22] and in designing constructs leading to improved efficiency in homology-directed repair.[23]

However, direct detection of Cas9 mediated DNA unwinding has been limited.[18,24] Work reported here uses the site-directed spin labeling (SDSL) technique to monitor conformational changes of a DNA duplex upon recognition by Cas9. SDSL employs electron paramagnetic resonance (EPR) spectroscopy to monitor stable radicals (*e.g.*, nitroxide spin labels) attached at specific sites of biomacromolecules and provides structural (*e.g.*, distance constraints) and dynamic (*e.g.*, motions at the labeling site) information on the parent molecules under physiological conditions.[25] In this work, R5a labels (Figure 1),[26] which belong to a family of nucleotide-independent nitroxide labels,[25] were attached at selected sites of a Cas9 target duplex without affecting Cas9 function. Inter-R5a distances were measured using double electron–electron resonance (DEER) spectroscopy[27] and were used in conjunction with all-atom molecular dynamics (MD) simulations to probe the bound DNA

Received: December 21, 2016
Accepted: April 24, 2017
Published: April 24, 2017

DOI: 10.1021/acschembio.6b01137
ACS Chem. Biol. 2017, 12, 1489–1493

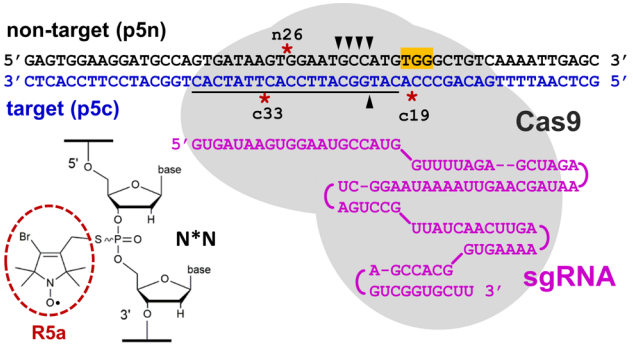

Figure 1. CRISPR−Cas9 system used for SDSL. Red asterisks (∗) indicate labeling sites of R5a (see inset). The PAM is highlighted in yellow. The protospacer is underlined, and DNA cleavage sites are marked by solid wedges.

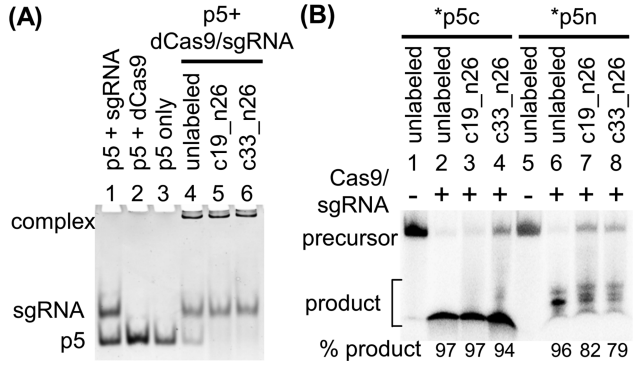

Figure 2. Biochemical characterization of R5a-labeled DNAs. (A) Complex formation characterized by native gel shift, visualized by ethidium bromide staining. Samples were assembled with a p5/sgRNA/protein ratio of 1:2:3 with [p5] = 0.5 μM, similar to EPR samples. (B) DNA cleavage detected by denaturing gel, visualized by autoradiography. The p5/sgRNA/protein ratio was 1:3:5 with [p5] = 0.1 μM. Purification tags on Cas9 were not removed, as they do not interfere with Cas9 function.[11] Excesses of sgRNA and Cas9 were used to ensure complete binding of target DNA but did not interfere with these results, as neither Cas9 nor sgRNA is capable of binding or cleaving the DNA (SI section S2.2.2).

conformations. The results support a model in which the unwound nontarget DNA strand is positioned along a positively charged patch located between the HNH and RuvC nuclease domains and reveal that strand scissions result in uneven increases in flexibility along the unwound nontarget DNA strand. These studies establish the synergistic combination of SDSL and MD to directly monitor Cas9-mediated DNA deformations and yield information regarding DNA conformations in different stages of Cas9 function. This will improve both the understanding of CRISPR−Cas9 mechanisms and the ability to customize its functionality.

Spin labeling studies were carried out on the *Streptococcus pyogenes* Cas9 system[4,28] (referred to hereafter as Cas9), with the target DNA duplex containing a 20-nucleotide (nt) protospacer [designated as p5, Figure 1; Supporting Information (SI) section S1]. On the basis of reported biochemical data,[11] R5a labels were attached, one at a time, at three sites: n26 of the nontarget strand and either c19 or c33 of the target strand (Figure 1). Following reported procedures,[4,28] sgRNA, wild type Cas9, and a catalytically inactive mutant (D10A and H840A, designated as dCas9) were produced (Figure S1). Specific binding of the unlabeled p5 duplex by the dCas9/sgRNA complex was detected by a native gel shift assay (Figure 2A, lanes 1−4; SI section S2.2.1). Furthermore, both doubly-R5a-labeled p5 duplexes, c19_n26 and c33_n26, were bound completely by the dCas9/sgRNA complex (Figure 2A, lanes 5 and 6; SI section S2.3), indicating that the doubly-R5a-labeled DNAs are recognized by Cas9.

Specific DNA cleavage by the Cas9/sgRNA complex was then tested (Figure 2B, SI section S2.2.2). For the unlabeled duplex, the target strand (p5c) was cleaved at a single site yielding a 22-nt ^{32}P-labeled product (Figure 2B, lane 2), while the nontarget strand (p5n) was cleaved at multiple sites yielding ^{32}P-labeled products estimated to be 30−33 nt (Figure 2B, lane 6). These cleavage patterns for both strands are consistent with previous reports.[4] With doubly-R5a-labeled duplexes, the R5a-labeled p5c strands were cleaved completely at a single site yielding a product the same size as that from the unlabeled p5c (Figure 2B, lanes 3 and 4), while the R5a-labeled p5n strands were cleaved nearly completely, yielding multiple products, similar to cleavage of the unlabeled p5n (Figure 2B, lanes 7 and 8). These data suggest that the simultaneous presence of two R5a labels at the sites specified here results in only small perturbations to DNA cleavage. Similar results were obtained for DNAs with a single R5a attached (SI section S2.2.3).

Following biochemical characterizations, continuous-wave (cw-) EPR spectroscopy was used to examine binding of singly-R5a labeled p5 duplexes by dCas9 (SI section S2.4). Consistent with the gel shift results, the presence of dCas9/sgRNA resulted in EPR spectral line broadening in all three singly labeled duplexes (Figure S6), indicating formation of the ternary complex. The bound DNA spectra with the label at n26 and c33 showed two components. The major components, which account for 75% and 82% of total spin population of n26 and c33, respectively, maintained the features of closely spaced splittings at the low- and high-field manifolds (Figure S7). This indicates that the majority of the label remains free of direct contact to either the protein or the RNA, and therefore inter-R5a distances measured on the doubly labeled c33_n26 duplex should report primarily DNA conformational changes upon interacting with Cas9. It is noted that the minor components of the n26 and c33 bound spectra (Figure S7), as well as the bound spectrum of c19 (Figure S6), showed characteristics of label immobilization. This indicates contacts between the label and the protein and/or RNA, which may give rise to the slightly better binding of the labeled DNA observed in the gel shift assay (Figure 2A). The impacts of these contacts on the pathway of DNA cleavage are not clear at this point, although they do not alter the final cleavage products (Figure 2B).

DEER measurements were then carried out on doubly labeled c33_n26 duplexes in different states (Figure 3, SI section S2.5). The unbound DNA revealed one population with a most probable distance of 21 Å (Figure 3A), which is consistent with the expected value from a canonical B-form duplex. In the presence of the dCas9/sgRNA complex, which binds and unwinds the DNA without cleavage, a clear change in the measured dipolar evolution trace was observed, and the resulting distance distribution showed a major population with a most probable distance of 27 Å (Figure 3B, SI section S2.6). This 6 Å increase in the inter-R5a distance is beyond the 10% experimental uncertainty of measured values (SI section S1.8) and reveals a deformation of the DNA duplex upon Cas9 binding.

DOI: 10.1021/acschembio.6b01137
ACS Chem. Biol. 2017, 12, 1489−1493

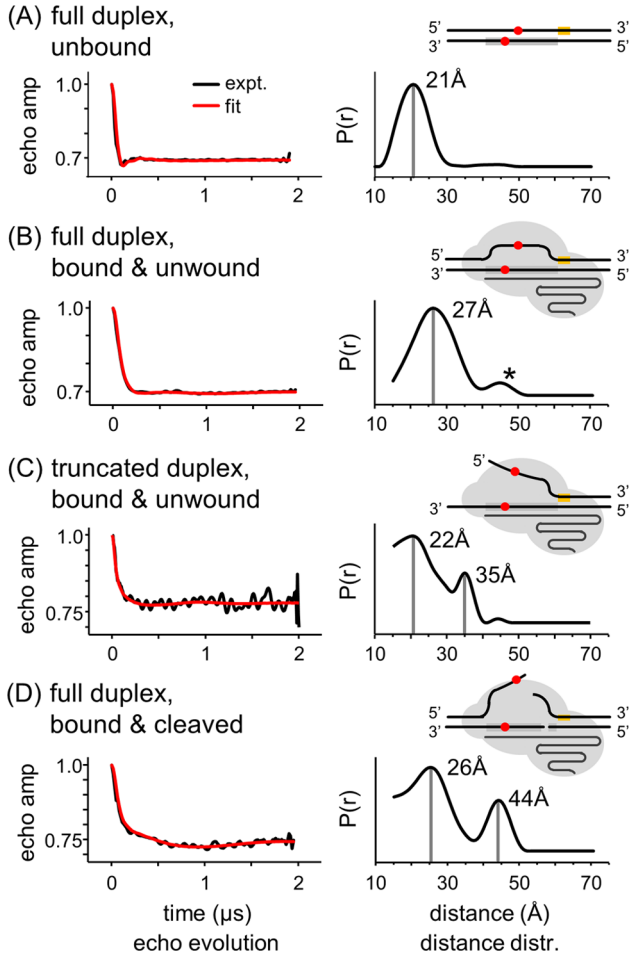

Figure 3. DEER measurements for the doubly-R5a-labeled c33_n26 duplex at various states. (A) Full duplex, unbound; (B) full duplex, bound and unwound; (C) truncated duplex, bound and unwound; and (D) full duplex, bound and cleaved. In each panel, the dipolar evolution trace is shown on the left, and the distance distribution is shown on the right. The asterisk (*) in panel B indicates an artifact (SI section S2.6). See also the additional DEER data in SI section S2.5.

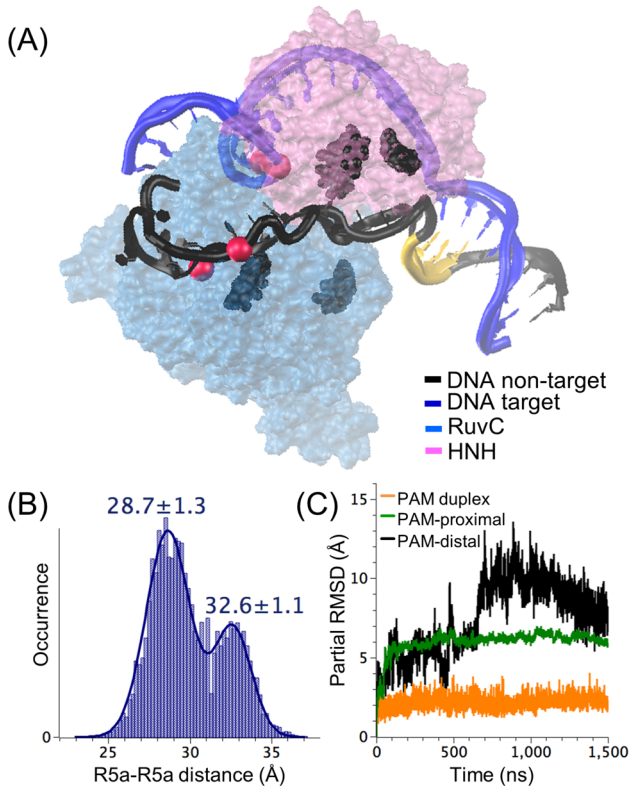

Figure 4. MD analysis of a Cas9 ternary complex model containing the unwound DNA. (A) Overlay of the two centroid structures of the most and second-most populated clusters. For clarity, only the nuclease domains (transparent surfaces) and the DNA strands (blue = target; black = nontarget; yellow = PAM) are shown. The red spheres indicate the P atoms to which the R5a labels are attached. Representative residues in the positively charged patch (K855 and K862 in HNH, H982 and K1047 in RuvC) are highlighted. (B) Histogram of distances between R5a labels modeled at the nucleotides equivalent to c33 and n26. (C) Partial RMSD traces for segments of the DNA nontarget strand with respect to the final snapshot of the minimization−equilibration phase (section S1.9). Nucleotides included to represent each segment are PAM duplex, −1 to −8 downstream of PAM; PAM-proximal, +1 to +8 upstream of PAM; PAM-distal, +12 to +16 upstream of PAM. See Figure S13 for more details.

In currently available cocrystal structures, the unwound nontarget DNA strand has been resolved up to only 9 nt upstream of the PAM,[18] which does not include the n26 R5a-labeling site. Therefore, the measured c33_n26 distance was evaluated using an atomistic model with the nontarget strand extended upstream of the PAM (Figure 4). The model was built from a Cas9 ternary structure containing 3 nt upstream of the PAM in the nontarget DNA strand (PDB ID 4UN3[13]), with the remaining nucleotides in the unwound nontarget strand initially reconstructed based on a hypothesis that the unwound nontarget strand is electrostatically stabilized at a positively charged patch between the HNH and RuvC nuclease domains.[21] After standard minimization−equilibration, the model was evolved for 1.5 μs in the presence of explicit water using all-atom MD simulations (SI section S1.9). Root-mean-square deviation (RMSD) analysis indicated that the overall ternary complex was stable over the 1.5 μs trajectory (Figure S11), and fluctuations in the conformations of the individual domains were clearly observed.

Using a previously validated NASNOX program[29,30] and regularly spaced snapshots from the MD trajectory, R5a labels were modeled onto the pair of nucleotides equivalent to n26 and c33 (SI section S1.9). The resulting c33_n26 distance distribution is bimodal (Figures 4B and S12). One subpopulation yielded an average R5a−R5a distance of 28.7 ± 1.3 Å, which is in good agreement with the DEER-measured value of 27 Å in the unwound full duplex (Figure 3B). On the other hand, the 32.6 Å population observed in the MD trajectory (Figure 4B) was not accounted for by the DEER data of the unwound full duplex (Figure 3B). Note that the MD model lacked the PAM-distal duplexed segment beyond the protospacer, which may afford higher flexibility in the DNA. To test this hypothesis, the c33_n26 distance was measured in a truncated p5 duplex in which the protospacer segment was no longer anchored by base-pairing at the PAM-distal side (Figure 3C, SI section S2.5). Indeed, the measured c33_n26 distance distribution became much broader in the 20−30 Å regime (Figure 3C), consistent with higher flexibility upon unwinding. Additionally, a new population centered at 35 Å was observed (Figure 3C), which reasonably accounts for the 32.6-Å population observed in MD simulations (Figure 4B).

DOI: 10.1021/acschembio.6b01137
ACS Chem. Biol. 2017, 12, 1489−1493

With SDSL measurements validating the equilibrated MD model, cluster analysis of the MD trajectory was carried out to examine conformations of the nontarget DNA strand (Figure 4 and SI section S2.7.3). The analysis revealed that while the nontarget strand was indeed localized in the vicinity of the positively charged patch during the entire trajectory, it showed substantially higher flexibility between the top two most populated clusters (Table S3) compared to the target strand, the sgRNA, or the HNH or RuvC nuclease domain (Figures 4A and S13). Furthermore, different segments of the nontarget strand showed variations in flexibility, as revealed by partial RMSD plots of individual segments (Figure 4C and Figure S13) and the contact maps generated based on distances between DNA nucleotides and protein residues located in the positively charged patch (Figures S14−S16). Specifically, the duplexed segment of the nontarget strand (PAM duplex, Figure 4C), which encompasses the PAM site (Figure S13A), showed low and stationary partial RMSD values throughout the trajectory. The data indicate the expected lower flexibility of the PAM duplex compared to the unwound single-stranded protospacer segment. In addition, within the protospacer, different dynamic characteristics were clearly observed between the PAM-distal and the PAM-proximal segments. The PAM-proximal segment showed a flat partial RMSD trace characterized by small fluctuations (Figure 4C). The PAM-distal segment showed sizable high-frequency fluctuations in its partial RMSD trace (Figure 4C), together with a large-scale transition at 450−700 ns (Figure 4C) that coincided with the transition from the second-most populated cluster to the most populated cluster (Table S3). These analyses indicate that the PAM-distal fragment is more flexible, and its conformational variations are largely responsible for structural evolutions in the nontarget strand. This conclusion on variable flexibility along the nontarget strand is further supported by the differences in the contact maps between the two most populated clusters (Figure S16). Overall, MD simulations support the model that the unwound nontarget strand is accommodated at the positively charged patch between the two nuclease domains[21] The results further reveal that scissions at the DNA backbone, which relax topological constraints, might result in differential increases in flexibility of the unwound nontarget strand.

The truncated duplex analyzed above (Figures 3C and 4) represents an engineered case that demonstrates enhanced DNA dynamics upon relaxing backbone topological constraints. A functionally relevant case of relaxed DNA topological constraints is the post-cleavage state, in which the DNA is cleaved and remains bound to the Cas9 complex for an extended period of time.[12] Using catalytically active Cas9, the c33_n26 distance was measured for this postcleavage state (Figure 3D). The resulting distance distribution profile revealed two major populations, centered at 26 and 44 Å (Figure 3D), both of which were determined to be statistically significant (SI section S2.6). As the majority of the DNA (>70%) was cleaved in the DEER sample (SI section S2.8), both distances are attributed to the cleaved DNA that remained bound by Cas9/sgRNA. The 26-Å subpopulation was the same, within the resolution of the measurement, as that observed in the dCas9-bound DNA (Figure 3B). While this could be interpreted as the DNA remaining in approximately the same conformation upon cleavage, additional distance measurements would be needed to confirm or dispute this conclusion. More interestingly, the appearance of a significant subpopulation centered at 44 Å clearly indicates a new DNA conformation upon cleavage. Given that the n26 label is located near the cleavage site on the nontarget strand (Figure 1), drifting of the nontarget strand upon cleavage may account for this much longer interspin distance. Data obtained with the active Cas9/sgRNA complex are consistent with reports that Cas9 undergoes conformational changes between target recognition (i.e., DNA binding and unwinding) and actual cleavage,[17,18] although their exact connections are not yet fully understood.

In summary, data presented here demonstrate the use of SDSL and MD to directly monitor alterations in DNA conformations as they interact with CRISPR−Cas9. Differences were detected between the unwound (i.e., dCas9-bound) and cleaved (i.e., Cas9-bound) states of the DNA. The data reveal that backbone scissions give rise to uneven increases in flexibility along the DNA nontarget strand. The results support a model in which the unwound nontarget DNA strand is stabilized by a positively charged patch between the HNH and RuvC domains of Cas9. The work establishes the SDSL/MD methodology in investigating conformational transitions within the large CRISPR−Cas9 complex and yields information regarding DNA conformations in different stages of Cas9 function. Coupled with spin-labeling of Cas9 proteins[31] and/or RNA, the SDSL/MD method will aid in deciphering the mechanisms of CRISPR−Cas9 recognition and specificity.

■ ASSOCIATED CONTENT

Supporting Information

The Supporting Information is available free of charge on the ACS Publications website at DOI: 10.1021/acschembio.6b01137.

Materials and Methods and additional data (PDF)

■ AUTHOR INFORMATION

Corresponding Author

*E-mail: pzq@usc.edu.

ORCID

Remo Rohs: 0000-0003-1752-1884

Peter Z. Qin: 0000-0003-3967-366X

Notes

The authors declare no competing financial interest.

■ ACKNOWLEDGMENTS

We thank L. Chen for help and advice on Cas9 expression and purification. Research reported was supported in part by the National Science Foundation (P.Z.Q., CHE-1213673), the National Institutes of Health (P.Z.Q., RR028992; R.R., R01GM106056 and U01GM103804), and the NVIDIA Corp. I.M.S. is supported by the Simons Center for the Social Brain.

■ REFERENCES

(1) Wiedenheft, B., Sternberg, S. H., and Doudna, J. A. (2012) RNA-guided genetic silencing systems in bacteria and archaea. *Nature 482*, 331−338.

(2) Sontheimer, E. J., and Barrangou, R. (2015) The Bacterial Origins of the CRISPR Genome-Editing Revolution. *Hum. Gene Ther. 26*, 413−424.

(3) Marraffini, L. A. (2015) CRISPR−Cas immunity in prokaryotes. *Nature 526*, 55−61.

(4) Jinek, M., Chylinski, K., Fonfara, I., Hauer, M., Doudna, J. A., and Charpentier, E. (2012) A Programmable Dual-RNA−Guided DNA Endonuclease in Adaptive Bacterial Immunity. *Science 337*, 816−821.

DOI: 10.1021/acschembio.6b01137
ACS Chem. Biol. 2017, 12, 1489−1493

(5) Gasiunas, G., Barrangou, R., Horvath, P., and Siksnys, V. (2012) Cas9−crRNA ribonucleoprotein complex mediates specific DNA cleavage for adaptive immunity in bacteria. *Proc. Natl. Acad. Sci. U. S. A. 109*, E2579−E2586.
(6) Cong, L., Ran, F. A., Cox, D., Lin, S., Barretto, R., Habib, N., Hsu, P. D., Wu, X., Jiang, W., Marraffini, L. A., and Zhang, F. (2013) Multiplex Genome Engineering Using CRISPR/Cas Systems. *Science 339*, 819−823.
(7) Mali, P., Yang, L., Esvelt, K. M., Aach, J., Guell, M., DiCarlo, J. E., Norville, J. E., and Church, G. M. (2013) RNA-Guided Human Genome Engineering via Cas9. *Science 339*, 823−826.
(8) Doudna, J. A., and Charpentier, E. (2014) Genome editing. The new frontier of genome engineering with CRISPR−Cas9. *Science 346*, 1258096.
(9) Hsu, P. D., Lander, E. S., and Zhang, F. (2014) Development and applications of CRISPR−Cas9 for genome engineering. *Cell 157*, 1262−1278.
(10) Nishimasu, H., Ran, F. A., Hsu, P. D., Konermann, S., Shehata, S. I., Dohmae, N., Ishitani, R., Zhang, F., and Nureki, O. (2014) Crystal Structure of Cas9 in Complex with Guide RNA and Target DNA. *Cell 156*, 935−949.
(11) Jinek, M., Jiang, F., Taylor, D. W., Sternberg, S. H., Kaya, E., Ma, E., Anders, C., Hauer, M., Zhou, K., Lin, S., Kaplan, M., Iavarone, A. T., Charpentier, E., Nogales, E., and Doudna, J. A. (2014) Structures of Cas9 Endonucleases Reveal RNA-Mediated Conformational Activation. *Science 343*, 1247997.
(12) Sternberg, S. H., Redding, S., Jinek, M., Greene, E. C., and Doudna, J. A. (2014) DNA interrogation by the CRISPR RNA-guided endonuclease Cas9. *Nature 507*, 62−67.
(13) Anders, C., Niewoehner, O., Duerst, A., and Jinek, M. (2014) Structural basis of PAM-dependent target DNA recognition by the Cas9 endonuclease. *Nature 513*, 569−573.
(14) Nishimasu, H., Cong, L., Yan, W. X., Ran, F. A., Zetsche, B., Li, Y., Kurabayashi, A., Ishitani, R., Zhang, F., and Nureki, O. (2015) Crystal Structure of Staphylococcus aureus Cas9. *Cell 162*, 1113−1126.
(15) Jiang, F., Zhou, K., Ma, L., Gressel, S., and Doudna, J. A. (2015) A Cas9−guide RNA complex preorganized for target DNA recognition. *Science 348*, 1477−1481.
(16) Josephs, E. A., Kocak, D. D., Fitzgibbon, C. J., McMenemy, J., Gersbach, C. A., and Marszalek, P. E. (2015) Structure and specificity of the RNA-guided endonuclease Cas9 during DNA interrogation, target binding and cleavage. *Nucleic Acids Res. 43*, 8924−8941.
(17) Sternberg, S. H., LaFrance, B., Kaplan, M., and Doudna, J. A. (2015) Conformational control of DNA target cleavage by CRISPR−Cas9. *Nature 527*, 110−113.
(18) Jiang, F., Taylor, D. W., Chen, J. S., Kornfeld, J. E., Zhou, K., Thompson, A. J., Nogales, E., and Doudna, J. A. (2016) Structures of a CRISPR−Cas9 R-loop complex primed for DNA cleavage. *Science 351*, 867−871.
(19) Singh, D., Sternberg, S. H., Fei, J., Doudna, J. A., and Ha, T. (2016) Real-time observation of DNA recognition and rejection by the RNA-guided endonuclease Cas9. *Nat. Commun. 7*, 12778.
(20) Fu, Y., Sander, J. D., Reyon, D., Cascio, V. M., and Joung, J. K. (2014) Improving CRISPR−Cas nuclease specificity using truncated guide RNAs. *Nat. Biotechnol. 32*, 279−284.
(21) Slaymaker, I. M., Gao, L., Zetsche, B., Scott, D. A., Yan, W. X., and Zhang, F. (2016) Rationally engineered Cas9 nucleases with improved specificity. *Science 351*, 84−88.
(22) Kleinstiver, B. P., Pattanayak, V., Prew, M. S., Tsai, S. Q., Nguyen, N. T., Zheng, Z., and Joung, J. K. (2016) High-fidelity CRISPR−Cas9 nucleases with no detectable genome-wide off-target effects. *Nature 529*, 490−495.
(23) Richardson, C. D., Ray, G. J., DeWitt, M. A., Curie, G. L., and Corn, J. E. (2016) Enhancing homology-directed genome editing by catalytically active and inactive CRISPR−Cas9 using asymmetric donor DNA. *Nat. Biotechnol. 34*, 339−344.
(24) Szczelkun, M. D., Tikhomirova, M. S., Sinkunas, T., Gasiunas, G., Karvelis, T., Pschera, P., Siksnys, V., and Seidel, R. (2014) Direct observation of R-loop formation by single RNA-guided Cas9 and Cascade effector complexes. *Proc. Natl. Acad. Sci. U. S. A. 111*, 9798−9803.
(25) Ding, Y., Nguyen, P., Tangprasertchai, N. S., Reyes, C. V., Zhang, X., and Qin, P. Z. (2015) Nucleic acid structure and dynamics: perspectives from site-directed spin labeling, In *Electron Paramagnetic Resonance*, pp 122−147, Royal Society of Chemistry.
(26) Popova, A. M., Kálai, T., Hideg, K., and Qin, P. Z. (2009) Site-Specific DNA Structural and Dynamic Features Revealed by Nucleotide-Independent Nitroxide Probes. *Biochemistry 48*, 8540−8550.
(27) Pannier, M., Veit, S., Godt, A., Jeschke, G., and Spiess, H. W. (2000) Dead-Time Free Measurement of Dipole-Dipole Interactions between Electron Spins. *J. Magn. Reson. 142*, 331−340.
(28) Anders, C., and Jinek, M. (2014) In Vitro Enzymology of Cas9, *Methods in Enzymology*, vol *546*, pp 1−20, Elsevier, DOI: 10.1016/B978-0-12-801185-0.00001-5.
(29) Qin, P. Z., Haworth, I. S., Cai, Q., Kusnetzow, A. K., Grant, G. P. G., Price, E. A., Sowa, G. Z., Popova, A., Herreros, B., and He, H. (2007) Measuring nanometer distances in nucleic acids using a sequence-independent nitroxide probe. *Nat. Protoc. 2*, 2354−2365.
(30) Tangprasertchai, N. S., Zhang, X., Ding, Y., Tham, K., Rohs, R., Haworth, I. S., Qin, P. Z., Peter, Z. Q., and Kurt, W. (2015) An Integrated Spin-Labeling/Computational-Modeling Approach for Mapping Global Structures of Nucleic Acids, *Methods in Enzymology*, vol *564*, pp 427−453, Elsevier, DOI: 10.1016/bs.mie.2015.07.007.
(31) Vazquez Reyes, C., Tangprasertchai, N. S., Yogesha, S. D., Nguyen, R. H., Zhang, X., Rajan, R., and Qin, P. Z. (2016) Nucleic Acid-Dependent Conformational Changes in CRISPR−Cas9 Revealed by Site-Directed Spin Labeling. *Cell Biochem. Biophys.*, 1−8.

DOI: 10.1021/acschembio.6b01137
ACS Chem. Biol. 2017, 12, 1489−1493